

A Novel Near-Land Radiometer Wet Path-Delay Retrieval Algorithm: Application to the Jason-2/OSTM Advanced Microwave Radiometer

Shannon Brown, *Member, IEEE*

Abstract—An algorithm is developed to retrieve wet tropospheric path delay (PD) near land from a satellite microwave radiometer to improve coastal altimetry studies. Microwave radiometers are included on ocean altimetry missions to retrieve the wet PD, but their performance has been optimized for retrievals in the open ocean. Near land, the radiometer footprint contains a mixture of radiometrically warm land and radiometrically cold ocean. Currently, the radiometer retrievals in the coastal region are flagged as invalid since large errors result when the open-ocean retrieval algorithm is applied to mixed land/ocean scenes. The PD retrieval algorithm developed in this paper is applicable to both open-ocean and mixed land–ocean scenes, thus enabling retrievals in the coastal zone. The performance of the algorithm is demonstrated with detailed simulations and application to measurements from the Advanced Microwave Radiometer on the Jason-2/Ocean Surface Topography Mission. The algorithm error is estimated to be less than 0.8 cm up to 15 km from land, less than 1.0 cm within 10 km from land, less than 1.2 cm within 5 km from land, and less than 1.5 cm up to the coastline.

Index Terms—Coastal altimetry, Jason-1, Jason-2/Ocean Surface Topography Mission (OSTM), land contamination, microwave radiometer, path delay (PD), satellite altimetry.

I. INTRODUCTION

SATELLITE altimeters have been used to precisely map ocean surface topography since the launch of the Topex/Poseidon (T/P) satellite in 1992. This time series of precision altimetry is continued by the Jason-1 and Jason-2/Ocean Surface Topography Mission (OSTM) satellites launched in 2001 and 2008, respectively. Other altimetry missions include Geosat, the Geosat follow-on (GFO), and the European ERS-1 and ERS-2 satellites with the Envisat follow-on. To accurately measure the sea-surface height, the range measured by the radar altimeter requires several corrections, one of them being a correction due to the delay of the radar signal as it propagates through the moist troposphere. The path delay (PD) of the radar signal due to water vapor can range from 0 to 50 cm and is highly variable in space and time [1]. Therefore, microwave radiometers operating near the 22-GHz water vapor absorption line have been included on all precision altimetry missions

to simultaneously determine the wet tropospheric PD, which is proportional to the integrated water vapor content of the atmosphere.

The radiometer is used to retrieve the wet PD in the open ocean with sufficient accuracy (errors of less than 1 cm), but this is not true near land. The statistical PD retrieval algorithm currently used to process the radiometer data for the Jason-1/2 altimeter missions is derived for pure ocean surfaces [1]. Other missions, such as GFO and ERS-1/2, use a similar retrieval algorithm [2], [3]. The ocean has an emissivity near 0.5 between 18 and 34 GHz, while land typically has an emissivity above 0.9 at these frequencies. Therefore, as the radiometer approaches the coast, the radiometrically warm land signal begins to fill the radiometer field of view and the retrieval errors rapidly increase. Currently, the radiometer measurement is flagged as invalid in the coastal region, thus impacting coastal studies using altimeter data. For the Topex Microwave Radiometer (TMR) on T/P and the Jason Microwave Radiometer (JMR) on Jason-1, the data are flagged as invalid starting from about 50 km from land [4], [5]. The Advanced Microwave Radiometer (AMR) on Jason-2/OSTM has about twice the spatial resolution and is flagged around 25 km from land. The land flag is triggered when the PD error due to land contamination becomes greater than about 5 mm. To improve coastal altimetry studies, a PD retrieval approach that is valid in the coastal region must be found.

Several approaches have been previously investigated to correct for the errors due to land contamination in microwave-radiometer retrieval algorithms [6], [7]. The approach used by [6] on Special Sensor Microwave Imager (SSM/I) data was to correct the brightness temperatures by removing the contribution from the land in mixed footprints. The uncontaminated brightness temperatures are then used directly with the open-ocean geophysical retrieval algorithms. This technique requires that the fraction of land in the radiometer field of view and the land brightness are known. The land fraction was estimated using the measured SSM/I antenna patterns along with a high-resolution land mask, and the brightness temperature of the land was estimated using nearby on-land measurements. The major error sources in this correction approach are uncertainties in the knowledge of the brightness temperature and uncertainties in the land fraction, arising from errors in the antenna pattern, land mask, or instrument navigation. For the case of SSM/I, it was found that navigation errors were the dominant source of error in the correction process.

Manuscript received April 3, 2009; revised August 27, 2009 and October 21, 2009. First published January 29, 2010; current version published March 24, 2010.

The author is with the Jet Propulsion Laboratory, California Institute of Technology, Pasadena, CA 91109 USA (e-mail: Shannon.T.Brown@jpl.nasa.gov).

Color versions of one or more of the figures in this paper are available online at <http://ieeexplore.ieee.org>.

Digital Object Identifier 10.1109/TGRS.2009.2037220

U.S. Government work not protected by U.S. copyright.

In [7], several land-contamination-correction approaches were investigated to particularly address the problem of retrieving PD in coastal regions for precision altimetry. Of the approaches tested, they found that the approach used by Bennartz [6] performed the best overall when applied to the case of TMR. The PD rms errors were estimated to be 2–3 cm in the coastal region using this approach, compared with 11–12 cm with no correction. These previous studies have exclusively focused on correcting the brightness temperatures, then applying the standard open-ocean retrieval algorithm. The approach discussed here is an all-together different approach to retrieve PD near land using an operationally simple algorithm. A simple fast algorithm is ideal for the near-real-time processing segment of operational altimetry.

The approach is motivated by the fact that the PD retrieval is most sensitive to the difference between the two channels on and off of the 22-GHz water vapor absorption line (18.7- and 23.8-GHz channels for the JMR and AMR and 18.0/21.0 GHz for the TMR) and that errors correlated between the two largely cancel in the retrieval process. The method of first correcting the brightness temperatures then implementing the open-ocean PD retrieval algorithm, while physically sound, acts to decorrelate the errors between the channels. The objective of this study is to develop a PD retrieval algorithm applicable to both pure ocean and mixed land/ocean scenes. The benefit of this approach, compared with correcting the brightness temperatures, is that many of the error sources are common to each channel and therefore offset in the retrieval algorithm. It also results in an operationally simple and computationally fast algorithm.

II. ALGORITHM DESCRIPTION

The radiometers on altimeter missions are nadir pointing and collocated with the altimeter footprint. The TMR operates at 18, 21, and 37 GHz and the JMR and AMR operate at 18.7, 23.8, and 34.0 GHz [4], [5]. The PD retrieval algorithm used by the TMR, JMR, and AMR, described in [1], uses a log-linear combination of the brightness temperatures with retrieval coefficients generated from a large database of modeled brightness temperatures. The algorithm is of the form

$$\text{PD}_{\text{GDR}} = c_0(\text{WS}_0, \text{PD}_0) + \sum_f c_f(\text{WS}_0, \text{PD}_0) \log(280 - T_B(f)) \quad (1)$$

where the retrieval coefficients c_0 and c_f are stratified by wind speed (WS) and PD and linearly interpolated by the algorithm to a first-guess PD (PD_0) and WS (WS_0). The PD computed in (1) is given the subscript *GDR* since this is the algorithm used for the altimeter Geophysical Data Record (GDR). The summation over frequency f refers to the three radiometer channels. The first-guess PD is determined using global coefficients valid for the entire PD range, and the first-guess WS is determined from the radiometer measurements using a simple statistical retrieval algorithm that takes the form of a linear combination of the brightness temperatures [1]. Stratifying the

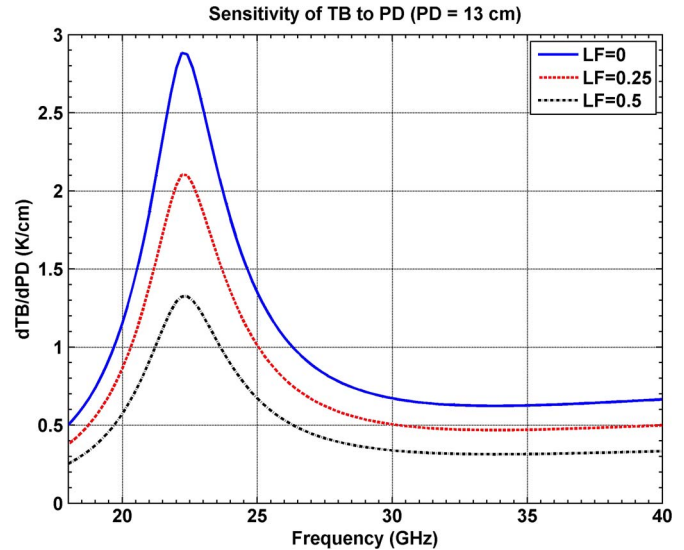


Fig. 1. Sensitivity of T_B to PD versus frequency for several land fractions.

coefficients by WS accounts for the nonlinear monotonically increasing dependence of the sea-surface emissivity with WS, which decreases the sensitivity of the top-of-atmosphere (TOA) brightness temperature (T_B) to PD.

Similarly, land emission will increase the measured brightness temperature above the open-ocean value according to the relationship

$$T_{\text{MB}}(f) = (1 - L_F(f)) T_{\text{Ocean}}(f) + L_F(f) T_{\text{Land}}(f) \quad (2)$$

where T_{MB} is the main-beam brightness temperature, L_F is the fraction of land in the radiometer main beam weighted by the antenna gain pattern, and T_{Ocean} and T_{Land} are the brightness temperatures of the ocean and land, respectively, and each term depends on the frequency. Using (2), along with a radiative transfer model (described in Section IV) to compute T_{Ocean} and T_{Land} , the sensitivity of the TOA T_B to PD for typical midlatitude conditions is computed for land fractions of 0, 0.25, and 0.5 and shown in Fig. 1. For this computation, the 1976 U.S. standard atmosphere was used. This computation was done by artificially perturbing the water vapor profile and finding the numerical derivative of brightness temperature with respect to PD. The sensitivity of the brightness temperature to PD decreases as the land fraction increases due to the increase in the background brightness, and hence, introduces a nonlinearity into the retrieval process. The decrease is greatest near the 22.235-GHz water vapor absorption line. There will also be an additional frequency dependence because the land fraction at a given distance from the coast decreases with increasing frequency. This is shown in Fig. 2, which shows the sensitivity of the JMR/AMR frequencies to PD versus the 18.7-GHz land fraction. The change in sensitivity at 23.8 GHz is nonlinear with respect to the 18.7-GHz land fraction, but would be linear with respect to the 23.8-GHz land fraction.

To the first order, the increase in the brightness temperature at a single frequency due to an increase in the WS in the open ocean is indistinguishable from that due to an increase in the

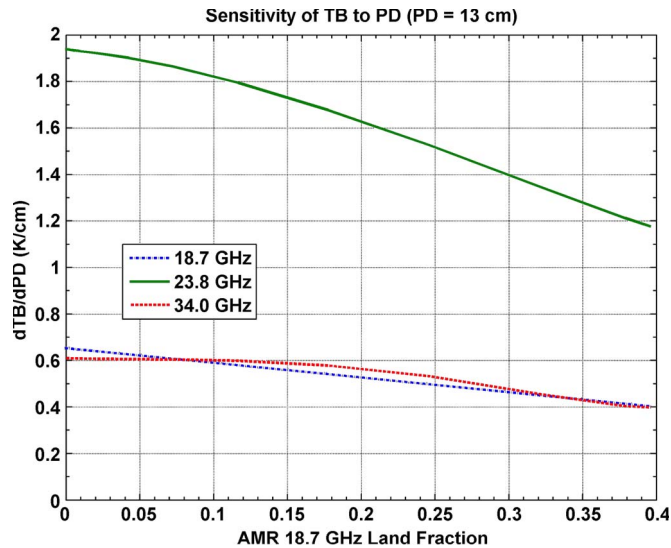


Fig. 2. Sensitivity of T_B to PD for the AMR frequencies as a function of the 18.7-GHz land fraction.

land fraction in the radiometer field of view when approaching the coast. Therefore, one can account for mixed land/ocean scenes in the algorithm in a manner similar to the way WS is treated in the open ocean. That is, the coefficients will be stratified based on the fraction of land in the radiometer footprint. Because the radiometer footprint changes with frequency, the coefficients are stratified by the land fraction in the main beam of the lowest frequency channel. This retrieval algorithm, which will be valid for open ocean and mixed land/ocean scenes, is called the mixed-pixel algorithm from this point forward and takes the form

$$PD_{MP} = c_0 (PD_0, L_F^{18.7}) + \sum_f c_f (PD_0, L_F^{18.7}) \log(280 - T_B(f)). \quad (3)$$

Like the GDR PD algorithm, the stratified coefficients are linearly interpolated to the land fraction value and the first-guess PD value to avoid discontinuities at the stratification boundaries. The additional stratification by WS was removed for the mixed-pixel algorithm. This was done in part because the WS algorithm is also invalid in the coastal region, meaning an ancillary WS estimate would be needed. It was also found that the performance impact of not including the WS stratification was minor, since the error is dominated by the emission from the land. In practice, the open-ocean algorithm (1) is used everywhere the land fraction is zero, and the mixed-pixel algorithm (3) is used everywhere the land fraction is greater than 0.01, and the two are merged by linearly interpolating between the two for land fractions greater than zero and less than 0.01. The land fraction threshold of 0.01 for switching between the two algorithms was chosen based on the observation that the error in the open-ocean algorithm begins to rapidly increase when the land fraction is greater than 0.01. This is described in more detail in Section IV.

III. ALGORITHM PARAMETERIZATION

The coefficients for the mixed-pixel algorithm are derived in a similar manner as the original PD coefficients [1]. The algorithm is parameterized using a large database of simulated coastal brightness temperature observations along with the corresponding wet tropospheric PD. To generate the simulated coastal brightness temperatures, three data sets are used; a large database of globally distributed open-ocean island radiosonde soundings, a statistical distribution of main-beam weighted land fractions for each channel, and a statistical distribution of land-surface brightness temperatures. The open-ocean island radiosonde observations are acquired from the Integrated Global Radiosonde Archive (IGRA) [8]. The quality-controlled radiosonde (RaOb) profiles acquired from the IGRA are additionally filtered to keep only the highest quality profiles for producing TOA T_B 's. The RaOb quality-control process is described in detail in [5]. The cloud model of [9] was used to generate cloud liquid-water profiles from the RaObs. The resulting database contained roughly 80 000 profiles and spanned the entire range of expected PD, WS, and cloud liquid-water conditions. The land fraction database is taken from the AMR land fraction map, which was computed by convolving the AMR main-beam antenna gain pattern with a high-resolution land mask (2' by 2'). The AMR main beam is defined as the region within 3° of the antenna boresight. For the AMR, this region contains roughly 98%–99% of the received power. The statistical distribution of coastal land-surface brightness temperatures is taken from the actual radiometer measurements that are made with the radiometer footprint completely over land.

A plane-parallel radiative transfer model is used to compute the TOA T_B 's using the RaOb profiles assuming an ocean scene, [T_{Ocean} in (2)]. The atmospheric gaseous absorption is determined using the oxygen absorption model of [10] and an updated version of the Liebe water vapor absorption model [11]. The cloud liquid-water absorption model is from [12]. The Stogryn [13] seawater dielectric model was used to compute the ocean surface emissivity. The 1976 U.S. standard atmosphere was used for heights above the maximum RaOb reading, and the sea-surface temperature was set to the temperature of the first reading in the profile. The humidity profile was extrapolated beyond the profile cutoff height, using an exponential fit to the radiosonde's humidity profile. The main-beam brightness temperature for a given land fraction is then computed using (2) by choosing a set of land fraction and land brightness temperature values from the respective databases.

For each model ocean T_B from the radiosonde database, a set of main-beam land fractions is randomly chosen from the land fraction database, and a set of T_{Land} values is randomly chosen from the land brightness temperature database based on the latitude of the radiosonde observation. To be considered a match, the latitude of the RaOb station had to be within 8° of the latitude of the measured land T_B . Here, a set refers to the three values for each of the AMR frequencies. The result is a large database of simulated coastal T_B observations along with wet PD computed from the radiosonde water vapor and temperature profiles. The mixed-pixel retrieval algorithm coefficients are

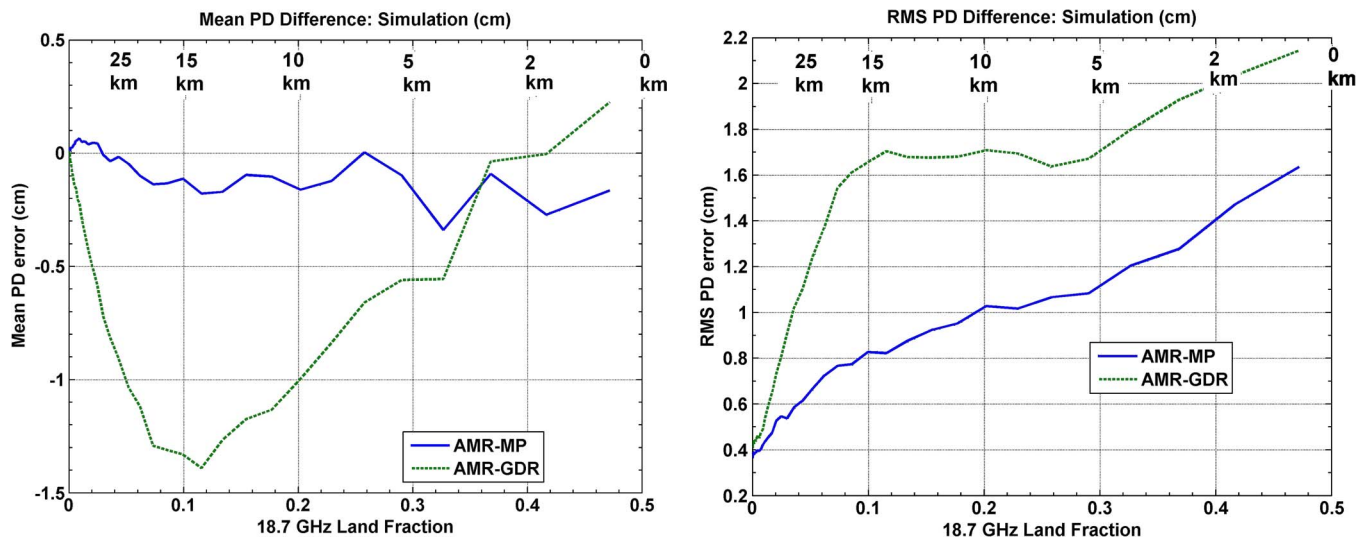


Fig. 3. (Left) Mean PD retrieval error and (right) rms error (retrieved minus simulated) as a function of the 18.7-GHz land fraction for the mixed-pixel and standard open-ocean (GDR) algorithms.

determined as a function of land fraction and PD range using least squares regression of the model T_B 's and PDs. This is done by separating the data into 22 land fraction ranges and four PD ranges. The PD ranges are 0–10 cm, 10–20 cm, 20–30 cm, and > 30 cm. A set of global coefficients valid for the entire PD range is also found for each land fraction stratification to compute the first-guess PD. The land fraction ranges are defined so that each roughly contained the same amount of simulated data. This means that the bin spacing is narrow for low land fraction values, and the bin spacing increases for higher land fraction values.

IV. SIMULATIONS

The algorithm performance is first estimated using a subset of the simulated coastal T_B 's database that was not used in the coefficient parameterization. The algorithm inputs are the simulated main beam T_B 's and the 18.7-GHz main-beam weighted land fraction. Gaussian distributed random noise with a standard deviation equal to the noise-equivalent delta temperature (NEDT) for each AMR channel was added to the simulated T_B 's. The AMR NEDTs are 0.12 K, 0.09 K, and 0.08 K, for the 18.7-, 23.8-, and 34.0-GHz channels, respectively [14]. A 10% relative error was assumed for the 18.7-GHz land fraction that is input to the algorithm. Contributors to this error are satellite navigation errors, land-mask errors, and errors in the measured antenna gain pattern. None of these sources of error is expected to be significant, and a 10% relative error is conservative. Regardless, the algorithm is fairly insensitive to land fraction errors since they are only used for choosing the coefficients that are discretely binned by land fraction.

For purposes of comparison, the simulated coastal T_B 's without any corrections applied are used with the standard open-ocean PD retrieval algorithm to simulate the errors that are present in the currently available product. The simulated retrieval errors for the GDR and mixed-pixel algorithms are binned by 18.7-GHz land fraction, and the results are plotted. Fig. 3 shows the mean and rms errors computed from

the simulations for the mixed-pixel and the GDR algorithms. Typical distances to land as a function of land fraction are noted at the top of the plot. The mixed-pixel algorithm exhibits no significant bias with increasing land fraction. The standard open-ocean algorithm has a characteristic bias that is a result of the 18.7-GHz channel first seeing land (reducing the 18-/23-GHz difference) followed by the remaining channels. The rms error for the mixed-pixel algorithm is observed to be below 1.2 cm up to a land fraction of 0.3, which corresponds to roughly a 5-km distance from land. The error is below 1 cm for land fractions of less than 0.2, or about 10 km from land. This is significantly lower than that predicted for the standard open-ocean algorithm, which has errors greater than 1.6 cm for land fractions greater than about 0.075, or about 20 km from land. For context, the mission requirement for the AMR is to retrieve the PD with an error of less than 1.2 cm, with a goal of 1.0 cm.

V. APPLICATION TO AMR DATA

The mixed pixel algorithm is applied to measured AMR data from July 2008 to February 2009. Direct validation of this type of retrieval is inherently difficult due to the scarcity of ground truth available in the coastal region. Therefore, the approach adopted is to show both a qualitative improvement by observing the algorithm output on a coastal approach and to use comparisons between AMR PDs and PDs predicted from the European Centre for Medium-Range Weather Forecasts (ECMWF) to validate the simulations. The algorithm error is then reported as that predicted from the simulations.

A. Qualitative Comparisons

Fig. 4 shows the AMR standard open-ocean PD, the PD from the mixed-pixel algorithm, and the ECMWF model PD as a function of distance to land as the satellite approaches the California coast near Point Conception (OSTM pass 43). This pass was chosen because it includes an overpass of the Harvest

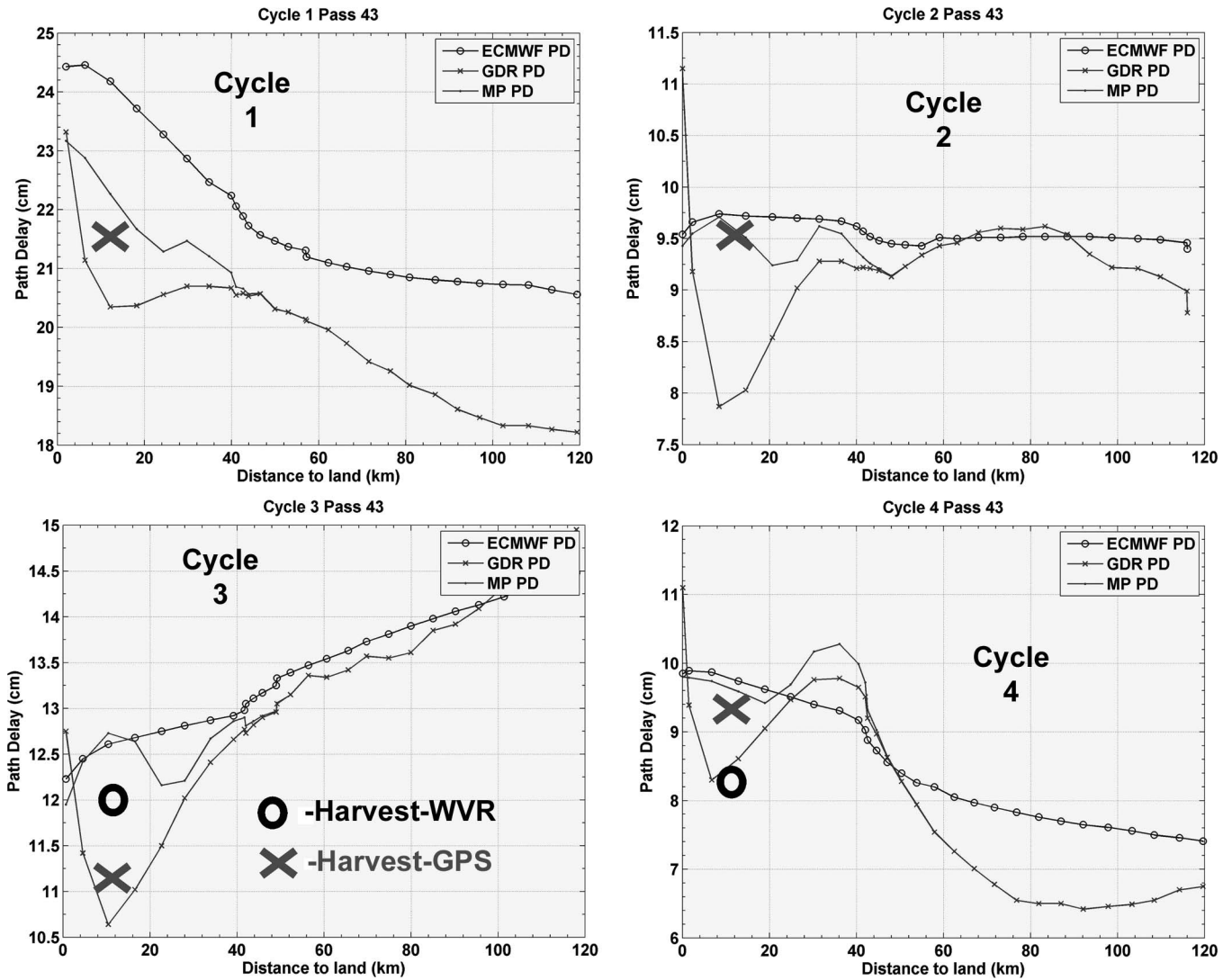


Fig. 4. AMR PD using standard algorithm and mixed-pixel algorithm for pass 43 near the California coast. The ECMWF model PD and that derived from the GPS and WVR at Harvest are also shown.

oil platform which has a GPS receiver and an upward looking water vapor radiometer (WVR) which provide independent PD estimates at the time of the overpass. The location of Harvest is 34.28 N, -120.41 E, placing it approximately 10 km from the coast. Data are shown for cycles 1–4. The GPS data were available for all cycles, and the WVR data were available for cycles 3 and 4. The GPS and WVR measured PDs are shown on the plot around 10 km from land. Up to a 1-cm difference is observed between the GPS and WVR measured PDs, illustrating the difficulty in validating the algorithm to the millimeter level using a small number of coastal PD measurements. Qualitatively, the mixed-pixel algorithm appears to perform better than the standard algorithm. This is based on the absence of the characteristic dip in the PD starting around 30 km from land that is present in the standard algorithm. In addition, the PD variations in the coastal zone indicated by the ECMWF model are better reflected by the mixed-pixel algorithm than the open-ocean algorithm. This is particularly evident in cycles 1 and 2.

B. Quantitative Comparisons With ECMWF PD

The AMR PDs are compared with PDs derived from the ECMWF model. The model fields are those that are included in the Jason-2 GDR. The mean and rms difference is found between AMR and ECMWF for the standard GDR algorithm and the mixed-pixel algorithm as a function of the 18.7-GHz land fraction. The results are shown in Fig. 5. A 0.4-cm constant bias, equal to open-ocean mean difference between ECMWF and the AMR PDs, is subtracted from the mean differences to better illustrate the additional PD error near land. Since the AMR PDs are not calibrated to ECMWF, an open-ocean bias at this level is not unexpected and within the absolute uncertainty of the radiometer calibration and retrieval algorithm. The signature of the mean difference approaching land for the GDR algorithm is very similar to that predicted by the simulations. The bias peaks around -1.3 cm at about 15 km from land. The mixed-pixel algorithm exhibits no significant bias from ECMWF approaching land. This also agrees with the simulations.

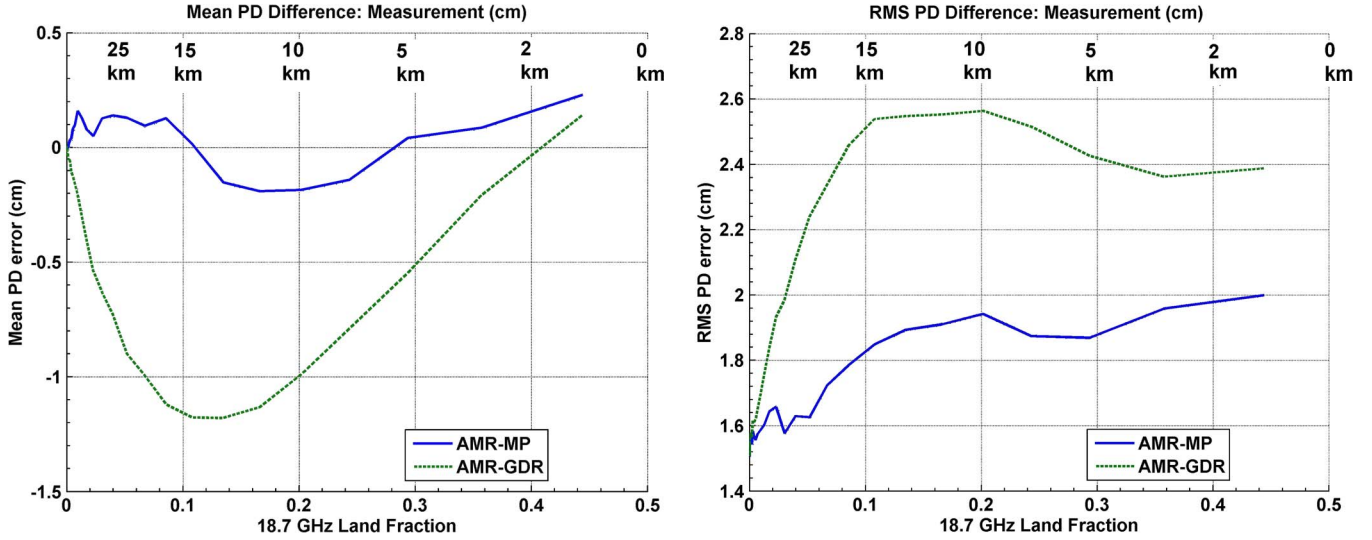


Fig. 5. Mean and rms of AMR minus ECMWF difference as a function of the 18.7-GHz land fraction.

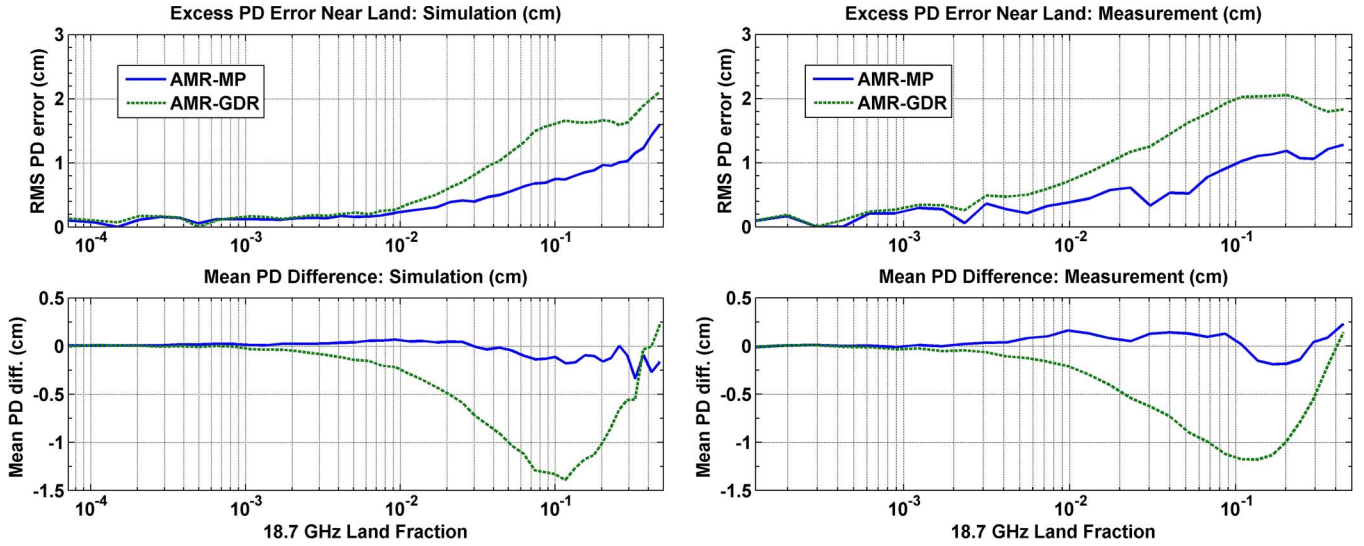


Fig. 6. Excess error near land predicted from the simulations and estimated from the AMR minus ECMWF comparisons.

The rms of the differences increases rapidly with increasing land fraction from about 1.6 cm to about 2.4 cm for the GDR algorithm. For the mixed-pixel algorithm, the rms error is much reduced for increasing land fraction. The error increases from 1.6 to 2 cm. The rms difference includes errors in both the radiometer retrieval and the ECMWF PD. To compare with the simulations, the rms difference for open-ocean scenes ($L_F = 0$) is removed to yield the excess rms error near land, using

$$\Delta PD_{\text{ALG}}(L_F) = \sqrt{\Delta PD_{\text{TOT}}(L_F)^2 - \Delta PD_{\text{TOT}}(L_F = 0)^2}. \quad (4)$$

The result is shown in Fig. 6 for the simulations and for the AMR–ECMWF comparisons. The top panel shows the excess PD error near land for the mixed-pixel and GDR algorithms. The bottom panel shows the bias approaching land, again with the open-ocean bias removed. The comparisons with ECMWF include the algorithm error plus residual model error in the coastal region. The error estimates from the simulations only include the algorithm error. Nevertheless, the two error esti-

mates are in good agreement, suggesting that the simulations accurately predict the algorithm error near land.

VI. CONCLUSION

A new algorithm has been developed to enable wet tropospheric PD retrievals near land from the microwave radiometers onboard ocean altimetry missions. The algorithm follows the form of the existing open-ocean PD retrieval algorithm developed for TMR/JMR/AMR, but is extended to be valid for mixed-pixel land/ocean scenes. This is accomplished by parameterizing the algorithm coefficients as a function of the 18.7-GHz land fraction using a database of modeled coastal T_B 's. The algorithm is valid globally up to a land fraction of 0.5, which corresponds to the antenna boresight centered on the coastline. A distinct advantage of the algorithm lies in its simplicity, in that it requires no dynamic ancillary data (such as land temperatures) and is computationally very fast. This makes it ideal for the near-real-time processing segment of the Jason-2/OSTM operational mission.

The algorithm error when applied to the AMR is estimated to be less than 0.8 cm up to 15 km from land, less than 1.0 cm within 10 km from land, less than 1.2 cm within 5 km from land, and less than 1.5 cm up to the coastline. This is estimated from detailed simulations and validated by comparisons with measured AMR data.

The algorithm developed is not particular to the AMR and can be applied to any other microwave radiometer to estimate integrated water vapor or wet PD in the coastal region, although the performance of the algorithm will likely be instrument particular, since it is dependent upon the antenna pattern of the radiometer. The mixed-pixel algorithm will next be applied to data from the JMR and the TMR.

ACKNOWLEDGMENT

The author would like to thank B. Haines for providing the Harvest GPS data, and S. Keihm for providing the Harvest WVR data. The work described in this paper was performed at the Jet Propulsion Laboratory, California Institute of Technology, under a contract with the National Aeronautics and Space Administration.

REFERENCES

- [1] S. Keihm, M. A. Janssen, and C. S. Ruf, "TOPEX/Poseidon Microwave Radiometer (TMR): III. Wet troposphere range correction algorithm and pre-launch error budget," *IEEE Trans. Geosci. Remote Sens.*, vol. 33, no. 1, pp. 147–161, Jan. 1995.
- [2] C. Ruf, R. Dewan, and B. Subramanya, "Combined microwave radiometer and altimeter retrieval of wet path delay for the GEOSAT follow-on," *IEEE Trans. Geosci. Remote Sens.*, vol. 34, no. 4, pp. 991–999, Jul. 1996.
- [3] L. Eymard, L. Tabary, E. Gerard, S. Boukabara, and A. Le Cornec, "The microwave radiometer aboard ERS-1: Part II—Validation of the geophysical products," *IEEE Trans. Geosci. Remote Sens.*, vol. 34, no. 2, pp. 291–303, Mar. 1996.
- [4] C. Ruf, S. Keihm, and M. A. Janssen, "TOPEX/Poseidon Microwave Radiometer (TMR): I. Instrument description and antenna temperature calibration," *IEEE Trans. Geosci. Remote Sens.*, vol. 33, no. 1, pp. 125–137, Jan. 1995.
- [5] S. Brown, C. Ruf, S. Keihm, and A. Kitiyakara, "Jason microwave radiometer performance and on-orbit calibration," *Mar. Geod.*, vol. 27, no. 1, pp. 199–220, Jan.–Jun. 2004.
- [6] R. Bennartz, "On the use of SSM/I measurements in coastal regions," *J. Atmos. Ocean. Technol.*, vol. 16, no. 4, pp. 417–431, Apr. 1999.
- [7] C. Desportes, E. Obligis, and L. Eymard, "On the wet tropospheric correction for altimetry in coastal regions," *IEEE Trans. Geosci. Remote Sens.*, vol. 45, no. 7, pp. 2139–2149, Jul. 2007.
- [8] I. Durre, R. S. Vose, and D. Wuertz, "Overview of the integrated global radiosonde archive," *J. Clim.*, vol. 19, no. 1, pp. 53–68, Jan. 2006.
- [9] C. Walcek and G. Taylor, "A theoretical method for computing vertical distributions of acidity and sulfate production within cumulus clouds," *J. Atmos. Soc.*, vol. 43, no. 4, pp. 339–355, Feb. 1986.
- [10] P. Rosenkranz, "Absorption of microwaves by atmospheric gases," in *Atmospheric Remote Sensing by Microwave Radiometry*, M. A. Janssen, Ed. New York: Wiley, 1993, ch. 2.
- [11] S. Cruz-Pol, C. Ruf, and S. Keihm, "Improved 20–32 GHz atmospheric absorption model," *Radio Sci.*, vol. 33, no. 5, pp. 1319–1333, Sep./Oct. 1998.
- [12] A. Benoit, "Signal attenuation due to neutral oxygen and water vapor, rain and clouds," *Microw. J.*, vol. 11, pp. 73–80, 1968.
- [13] A. Stogryn, "Equations for calculating the dielectric constant of saline water," *IEEE Trans. Microw. Theory Tech.*, vol. MTT-19, no. 8, pp. 733–736, Aug. 1971.
- [14] A. Kitiyakara, S. Brown, and R. Manvi, "OSTM Advanced Microwave Radiometer (AMR) thermal vacuum test report," JPL Project Doc. JPL D-32417, Dec. 20, 2005.



Shannon Brown (S'01–M'05) received the B.S. degree in meteorology from the Pennsylvania State University, University Park, and the M.S. degree in atmospheric science and, in 2005, the Ph.D. degree in geoscience and remote sensing from the University of Michigan, Ann Arbor.

Since 2005, he has been with the Jet Propulsion Laboratory, California Institute of Technology, Pasadena, as a member of the engineering staff in the Microwave Advanced Systems Section, where he is currently a Senior Engineer. He is also currently the Instrument Scientist for the NASA Juno Microwave Radiometer. He has been involved with the spaceborne Topex and Jason Microwave Radiometers, WindSat Polarimetric Radiometer, and the Jason follow-on Advanced Microwave Radiometer. His research interests include microwave radiometer calibration and geophysical algorithm development for both passive and active sensor.

Dr. Brown is the recipient of the NASA Exceptional Achievement Medal in 2009 for contributions to the OSTM Advanced Microwave Radiometer as well as three NASA Group Achievement Awards.